Published in final edited form as:
Circ Res. 2012 February 17; 110(4): 551–559. doi:10.1161/CIRCRESAHA.111.255927.

Left-Right Symmetry Breaking in Tissue Morphogenesis via Cytoskeletal Mechanics

Ting-Hsuan Chen, **Jeffrey J. Hsu**, **Xin Zhao**, **Chunyan Guo**, **Margaret Wong**, **Yi Huang**, **Zongwei Li**, **Alan Garfinkel**, **Chih-Ming Ho**, **Yin Tintut**, and **Linda L. Demer**
Mechanical and Aerospace Engineering Department (T.-H.C., Y.H., C.-M.H.), Department of Medicine (J.J.H., A.G., Y.T., L.L.D.), Department of Bioengineering (M.W., C.-M.H., L.L.D.), and Department of Integrative Biology and Physiology (A.G., L.L.D.), University of California Los Angeles, Los Angeles, California, USA; Institute of Robotics & Automatic Information System (X.Z., C.G., Z.L.), Nankai University, Tianjin, China.

Abstract

Rationale—Left-right (LR) asymmetry is ubiquitous in animal development. Cytoskeletal chirality was recently reported to specify LR asymmetry in embryogenesis, suggesting that LR asymmetry in tissue morphogenesis is coordinated by single- or multi-cell organizers. Thus, to organize LR asymmetry at multiscale levels of morphogenesis, cells with chirality must also be present in adequate numbers. However, observation of LR asymmetry is rarely reported in cultured cells.

Objectives—Using cultured vascular mesenchymal cells, we tested whether LR asymmetry occurs at the single cell level and in self-organized multicellular structures.

Methods and Results—Using micropatterning, immunofluorescence revealed that adult vascular cells polarized rightward and accumulated stress fibers at an unbiased mechanical interface between adhesive and non-adhesive substrates. Green fluorescent protein transfection revealed that the cells each turned rightward at the interface, aligning into a coherent orientation at 20° relative to the interface axis at confluence. During the subsequent aggregation stage, time-lapse videomicroscopy showed that cells migrated along the same 20° angle into neighboring aggregates, resulting in a macroscale structure with LR asymmetry as parallel, diagonal stripes evenly-spaced throughout the culture. Removal of substrate interface by shadow mask-plating, or inhibition of Rho kinase or non-muscle myosin attenuated stress fiber accumulation and abrogated LR asymmetry of both single cell polarity and multicellular coherence, suggesting that the interface triggers asymmetry via cytoskeletal mechanics. Examination of other cell-types suggests that LR asymmetry is cell-type specific.

Conclusions—Our results show that adult stem cells retain inherent LR asymmetry that elicits *de novo* macroscale tissue morphogenesis, indicating that mechanical induction is required for cellular LR specification.

Correspondence to: Linda L. Demer Department of Medicine, University of California Los Angeles 10833 LeConte Avenue Los Angeles, CA 90095-1679 Phone: (310) 206-2677 (office) FAX: (310) 825-4963 Ldemer@mednet.ucla.edu.

Disclosures
None.

Keywords

Adult stem cells; Cell culture; Development; Migration; Morphogenesis

Introduction

Left-right (LR) asymmetry often occurs in embryonic and tissue morphogenesis, such as helices of snail shells and internal organs in most extant metazoan animals.[1] In some vertebrates, LR asymmetry is believed to be generated by motile cilia, whose beating generates a leftward fluid flow to step up downstream morphogen gradients. Another model is that LR asymmetry is motivated by intracellular events originated by cytoplasmic organization at an even earlier stage.[2] Recently, cytoskeletal chirality and planar cell polarity were shown to specify the LR axis at early embryogenesis,[3-6] suggesting that LR asymmetry is coordinated by single- or multi-cell organizers and propagates through the rest of the tissue architecture,[7] as evidenced by epithelial cell chirality underlying the hindgut rotation[8] and chiral movement of blastomeres.[6] Thus, to organize LR asymmetry at multiscale levels of morphogenesis, cells with chirality must also be present in adequate numbers. However, although LR asymmetry is ubiquitous, from whole-body and visceral handedness to myocyte fiber orientation, chiral behavior from non-embryonic cells after enzymatic isolation in culture has been seen rarely in past decades.

To investigate such LR asymmetry and cellular chirality, we cultured vascular mesenchymal cells (VMCs) on a micropatterned substrate. VMCs differentiate and self-organize into periodic multicellular aggregates resembling patterns in normal tissue architecture. We report that, on migration across an interface between adhesive and non-adhesive substrates in culture, VMCs preferentially turn right and self-organize into periodic multicellular structures with remarkably consistent alignment on the principal diagonal axis. This *de novo* LR asymmetry in non-embryonic cells required stress fiber accumulation on encountering the substrate interface, suggesting that mechanical induction, possibly resembling contextual instruction from native tissue architectures, is required to regain chirality in culture for morphogenesis after cells are enzymatically isolated from their native tissue.

Methods

Micropatterning

A glass substrate with hexamethyldisilazane (HMDS) and polyethylene glycol (PEG) substrate was prepared as described previously. Prior to plating cells, the HMDS/PEG substrates were first incubated with solutions of extracellular matrix (ECM), consisting of fibronectin (FN), collagen types I and IV, or laminin-1, to allow adsorption on HMDS. The protein-coated chip was then plated with VMCs, bovine vascular endothelial cells (BVECs), NIH 3T3 fibroblast (3T3) or mouse bone marrow stromal cell line (ST2) with brief washings such that only cells adhering to the ECM regions remained.

Shadow-mask plating

The mask was made of stainless steel (2 cm × 2 cm × 100 μm, NW Etch, WA) containing 25 parallel windows (300 μm × 1.5 cm) spaced 300 μm apart. Prior to plating, the tissue culture dish was first uniformly coated with FN solution. Thereafter, cells were plated through the mask followed by removal of the shadow-mask.

Cell culture

VMCs, BVECs, and 3T3 cells were isolated and cultured as described[9-11] and ST2 cells were commercially purchased (Cell Bank, Riken Bioresource Center, Japan). All cells were grown in Dulbecco's Modified Eagle's Medium supplemented with 15% heat inactivated fetal bovine serum and 1% penicillin/streptomycin (10,000 I.U./10,000 μg/ml; all from Mediatech, Inc., VA). Cells were incubated at 37° C in a humidified incubator (5% CO_2 and 95% air) and passaged every three days.

Multicellular pattern formation

Each culture was prepared on one of four substrates: 1) 35-mm plastic dishes, 2) binary substrates consisting of PEG alternating with purified ECM protein (FN, collagen I, collagen IV, or laminin-1), 3) uniformly coated FN substrate on chips with titanium markers on the reverse side of chip, or 4) shadow-mask plating as described elsewhere in methods, with media changes every three days. For inhibition of stress fibers or intervention of morphogen activities, Y27632, blebbistatin, bone morphogenetic protein-2 (BMP-2), noggin, and warfarin were added at day zero and replenished with each media change. After 10-14 days, cultures were stained with hematoxylin to reveal multicellular aggregates.

Green fluorescent protein transfection

VMCs were transfected with a plasmid encoding green fluorescent protein (GFP) (pmaxGFP; Amaxa Biosystems, Germany) using the Effectene Transfection Reagent (Qiagen, CA).

Time-lapse videomicroscopy

Cultures were incubated in a microscopic thermal stage (HCS60, Instec, Inc., CO) at 37° C and continuously supplied with premixed 5% CO_2. Images were acquired at 5 min intervals for a total of 22.5 hours using charge-coupled devices (CCD) and an inverted microscope in bright field.

Immunofluorescent staining

Cells were cultured on FN/PEG substrates or shadow-mask plated in normal growth medium, or on FN/PEG substrates in growth medium supplemented with Y27632 or blebbistatin. Cells were fixed in cold methanol, blocked with Image-iT™ FX signal enhancer (Invitrogen, CA) at room temperature, then labeled with monoclonal anti-α-tubulin-FITC antibody (Sigma-Aldrich, St. Louis, MO; 1:50; for polarity assay on VMCs and BVECs), pericentrin polyclonal antibody (Covance, CA; 1:500; for polarity assay on 3T3 cells and ST2 cells), or non-muscle myosin-IIa (NMM-IIa) antibody (Covance, CA; 1:1000; for stress fiber distribution on all cell types) at room temperature for 1 hour. The pericentrin and NMM-IIa antibodies were subsequently labeled with appropriate secondary antibodies. Samples were mounted with DAPI. For stress fiber distribution of NMM-IIa, images were stacked using etched microgrooves on the reverse surface for registration. For shadow-mask plating experiments, images were stacked using automated edge detection for registration.

Orientation analysis

Images were processed by segmentation and boundary tracing to allow the identification of cells based on the size of the closed-loop regions. The orientation angle was calculated by the method of “minimum circumscribed rectangle” in which the shape of a given cell can be approximated by circumscribing rectangles of different sizes. The orientation angle, θ, was defined as the longitudinal axis of the rectangle of minimal area relative to the horizontal axis of the image (and of the interface).

Stacking images of immunofluorescence NMM-IIa after shadow-mask plating

Images were processed by segmentation and boundary tracing to binarize the image and identify the sheet of cells by excluding small closed-loop regions. We selected a level of 300 bright pixels per row as the threshold to identify the edge of the cell sheet. The midline of the cell sheet, defined as equidistant between two edges, was used to register and stack the images.

Mathematical model

See Online Data Supplement for details.

Results

LR asymmetry in pattern formation of vascular mesenchymal cells

VMCs, when homogeneously plated on conventional tissue-culture plastic, aligned locally with their neighbors at confluence (Figure 1A). After 2 weeks, they differentiated and self-organized into periodic aggregates in labyrinthine configurations as seen in reaction-diffusion phenomena (Figure 1C)[9, 12-16]. To test effects of initial plating distribution, we micro-engineered glass substrates with functional surfaces composed of alternating stripes (300 μm-wide) of cell-adhesive FN and non-adhesive PEG (Figure 1B; black stripes = titanium lines on reverse side indicating FN/PEG interfaces).[17] After one week, cells spread beyond the FN onto the PEG regions toward confluence. After 10-14 days, instead of the expected labyrinthine pattern, cells aggregated into long, straight, and parallel ridges, consistently aligned on a principal diagonal relative to the interfaces – a striking, unidirectional LR asymmetry (Figure 1D). Of note, the formation of ridges with LR asymmetric alignment was independent of passage number for P16 to P26. For example, Online Figure I E and I F, and Figure 1D are from 3 different passages. It was also unaffected by treatments with BMP-2, noggin (BMP-2 inhibitor), or warfarin (inhibitor of matrix gamma-carboxyglutamic acid protein (MGP)) (Online Figure I A to D). Furthermore, it was unaffected by substituting other cell-adhesive substrata in lieu of FN (Online Figure II).

Coherent single-cell orientation perpendicular to the axis of diagonal ridges directing the subsequent migration toward aggregates

To study earlier stages of this novel asymmetry, individual VMCs were tracked by GFP transfected at low-efficiency. At confluence, cells oriented coherently and consistently in an anti-diagonal direction. This angle of cell orientation, θ, was defined relative to the titanium lines (Figure 2A). From days 2-5, mean θ increased and its standard deviation decreased ($6 \pm 30° \rightarrow 19 \pm 14°$, Figure 2C and Online Figure III), indicating a coherent orientation toward an angle perpendicular to the alignment of multicellular ridges ($\theta + 90° = \sim 110°$, Figure 1D). This cell orientation appeared earlier on FN then later on PEG, ultimately occurring throughout the plate (Online Figure IV). On plates with wider (300-600 μm) FN/PEG stripes, cells also oriented coherently with the same angle (Online Figure V). In contrast, on uniform FN substrates, cells oriented randomly (Figure 2B and 2D). Thus, the coherent orientation of individual cells perpendicular to multicellular ridges seems to be dependent on the presence of FN/PEG interface but independent of the interface spacing.

In addition, to assess tightness of the control of cell orientation by interface angle, we created two orthogonal sets of interfaces on the same chip (Online Figure VI A and VI B) and found that multicellular aggregates aligned in a stripe pattern at 110° relative to the local interfaces up to a transition zone (~300 μm wide) at the junction, where cell alignment smoothly curved and nodules arose (Online Figure VI C and VI D). These results indicate the importance of substrate interface orientation.

To test whether the coherent orientation contributes to ridge formation, time-lapse videomicroscopy was performed at confluence to capture the time course of LR alignment. Cells migrated toward discrete aggregates preferentially following the coherent orientation θ, and gradually formed parallel ridges aligned at $\theta + 90°$ (Figure 3 and Online Video I). This suggests that the coherent orientation guides and constrains migration direction, resulting in multicellular ridges along the principal diagonal. Of note, ridge formation was simultaneous on both FN and PEG substrates for most experiments, but occurred earlier on FN in the time-lapse, possibly due to the required frequent media changes for the thermal stage. We also noted that, although the multicellular ridge alignment was independent of ECM, there was a subtle increase in coherence and uniformity of θ for cells on collagen IV (orientation angle: collagen IV, 22 ± 7°; collagen I, 25 ± 15°; laminin-1, 28 ± 17°; mean ± s.d., n > 500 each), as demonstrated by its smaller standard deviation.

To study how reaction-diffusion together with preferential migration could give rise to parallel ridges with asymmetric alignment, we developed a mathematical model. The activities of a slowly-diffusing activator, BMP-2, u, its rapidly-diffusing inhibitor, MGP, v, and cell density, n, reflecting proliferation, cytokinetic diffusion and chemotactic migration toward activators, were modeled as functions of a 2-dimensional domain (x, y) following reaction-diffusion kinetics:[14, 18, 19]

$$\begin{aligned}
&\frac{\partial u}{\partial t^*} = D\nabla^{*2}u + \gamma\left(\frac{nu^2}{v(1+ku^2)} - cu\right)\\
&\frac{\partial v}{\partial t^*} = \nabla^{*2}v + \gamma\left(nu^2 - ev\right)\\
&\frac{\partial n}{\partial t^*} = \sum_{ij} A_{ij}\left[\nabla^{*T} \otimes \left(D_n\nabla^* n - \frac{\chi_0 n}{(k_n+u)^2}\nabla^* u\right)\right]_{ij} + r_n n(1-n)\\
&A = \begin{bmatrix} b_1\cos^2\theta + b_2\sin^2\theta & (b_1-b_2)\cos\theta\sin\theta \\ (b_1-b_2)\cos\theta\sin\theta & b_1\sin^2\theta + b_2\cos^2\theta \end{bmatrix}
\end{aligned} \qquad (1)$$

where D is the ratio of activator to inhibitor diffusion coefficients; D_n is the ratio of cytokinetic to inhibitor diffusion coefficients; k is the coefficient of autocatalytic saturation; γ is a scaling factor related to domain size, biosynthetic timescale, and inhibitor diffusivity; c and e are degradation terms; χ_0 and k_n are chemotactic migration coefficients; r_n is the proliferation rate. We used adjustable coefficients, b_1 and b_2, to model differential migration rates along the principal axes, described as vectors ($\cos\theta$, $\sin\theta$) and ($-\sin\theta$, $\cos\theta$) (Figure 4A), whereas the parameters of the chemical kinetics of BMP-2 and MGP were held constant in the simulations given the experimental finding that addition of morphogens did not inhibit emergence of LR asymmetry (Online Figure I A to D). For more detailed description of mathematical derivation and parameter estimation, see Online Data Supplement.[14, 18-21] Initial conditions were uniformly distributed u, v, and n with 2% random perturbations. For isotropic migration ($b_1 = b_2 = 1$), the simulation produced labyrinthine patterns of $n(x, y)$ over the computational domain (Figure 4B and Online Video II). For anisotropic migration ($b_1 = 1$, $b_2 = 10^{-6}$, $\theta = 20°$), the simulation produced diagonal stripes aligned at $\theta + 90°$ (Figure 4C and Online Video III), consistent with the multicellular diagonal ridges in our experiments. Thus, the model verifies that reaction-diffusion, together with anisotropic migration guided by coherent orientation, account for the development of unidirectional ridges.

LR polarity is associated with stress fiber accumulation in VMCs at FN/PEG interface

Since intracellular polarization of the cell-motility apparatus directs migration,[22-24] it may also explain the coherent orientation and migration of VMCs. Just as cells at the leading edge of a “wound” are polarized with their microtubule organizing centers (MTOC) facing the wound,[25, 26] VMCs may also polarize with their MTOC facing the bare PEG substrate (outward from the FN stripes). We reasoned that, if the MTOC also had a LR polarization

accompanying outward polarity, it might account for the orientation angle θ. We visualized the MTOC by α-tubulin immunofluorescence and classified its polarity relative to the nucleus centroid (Online Figure VII) into quadrants of Right/Out, Right/In, Left/Out and Left/In for cells past, near or ≥120 μm remote from the FN edge (Figure 5A). Six hours after plating, significantly more cells that were past the interface polarized towards Right/Out compared with cells remote from the FN edge (Figure 5B) ($p < 0.0001$, Fisher's Exact Test). This was seen as early as 2 hours after plating (Figure 5C). While outward polarization is consistent with known cell behavior in wound healing,[25, 26] the rightward preference is novel. In addition, there was a gradient of increasing polarization as the cells approached and passed the interface (Figure 5B), possibly due to the propagation of biased polarity by cell-cell interaction. As expected, this right-turning relative to outward migration occurred at both edges of a FN stripe. Thus, intracellular compartmental polarization, specifically the MTOC relative to the nuclear centroid, appears to contribute to the development of coherent orientation.

Preferential outward migration competes with haptotaxis, which tends to retain cells on FN adhesion sites. Given that actomyosin contractility is required for cell migration, we hypothesized that cells encountering the non-adhesive PEG assembled additional actomyosin stress fibers, thereafter triggering the expression of LR polarity. We visualized stress fiber distribution by immunofluorescence of NMM-IIa 6 hours after plating (Figure 6A).[27, 28] Image stacking, with registration to create a heat map of local stress (n = 45),[28, 29] showed accumulation of actomyosin stress fibers at the FN/PEG interface (Figure 6B). Inhomogeneous cell distribution was excluded by nuclear staining (Figure 6C and 6D; single and stacked images). Since accumulation of stress fibers is localized at FN/PEG interfaces, resembling the spatial distribution of LR polarity, it may contribute to the LR polarity gradient.

Abrogation of LR polarity and multicellular alignment with removal of interface or inhibition of stress fiber accumulation

To test whether the stress fiber accumulation and LR polarity are associated with FN/PEG interfaces, but not with inhomogeneous cell-cell contacts, we used an additional method to restrict cell plating to specific regions. A thin shadow-mask, containing 25 long, rectangular windows, was overlaid on a homogeneous FN substrate before plating cells. The mask was removed after 30 minutes, leaving cells only within the 25 rectangular domains ((Figure 7A and Online Figure VIII). After 6 hours, cells at the edge of cell sheets polarized outward, but showed no LR polarity (Figure 7B) or stress fiber gradient (Figure 7C). After 14 days, consistent with the lack of LR polarity or stress fiber gradient, the multicellular ridges failed to produce parallel ridges along the principal diagonal, instead, forming a labyrinthine pattern as in conventional cultures (Figure 7D). Thus, the FN/PEG interface is essential for expression of stress fiber accumulation, LR polarity and multicellular aggregates with asymmetric alignment.

To further test whether stress fiber accumulation is required for LR polarity, we used the non-muscle myosin-II inhibitor, blebbistatin, and the Rho kinase (ROCK) inhibitor, Y27632, to inhibit stress fiber accumulation specifically on non-muscle myosin-II phosphorylation in response to Rho kinase.[27-30] In the presence of either inhibitor, results showed loss of stress fiber accumulation (Figure 8A and 8B), loss of LR polarity of cells near the interface (Figure 7B), and loss of the coherent orientation (Online Figure IV B and IV C). In addition, the multicellular aggregates failed to exhibit asymmetric alignment, instead, forming a labyrinthine pattern in the presence of Y27632 and a more disorganized pattern in the presence of blebbistatin (Figure 8C and 8D).

To test for cell-type specificity, BVECs, 3T3 cells and ST2 cells were cultured on the FN/PEG substrates. Stress fiber accumulation at the interface was seen in all cell types, but ST2 cells showed leftward-biased polarity whereas BVECs and 3T3 cells showed neutral polarity near the interface (Online Figure IX). Since ST2 cells are multipotent but do not self-assemble into aggregates under our culture conditions, it suggests that LR asymmetry is not tied to self-assembly but possibly to multipotency. Together with results that inhibition of stress fiber formation abrogated LR polarity and the alignment of VMC aggregate patterns, it indicates that cytoskeletal reorganization is necessary and cell-type specific for the LR asymmetry.

Discussion

Our findings suggest an inherent, cryptic chirality in VMCs that is revealed by an unbiased extracellular mechanical transition and mediated by cytoskeletal reorganization, analogous to chemically-induced chirality seen in neutrophil-like cells.[31] To our knowledge, this is the first demonstration of an association between LR asymmetry and cytoskeletal reorganization, triggered by an unbiased mechanical interface, and the first demonstration that a microscale dynamic asymmetry unfolds into a *de novo*, consistently oriented and periodic macroscale pattern resembling tissue architecture. In VMCs, the rightward-biased turning required stress-fiber accumulation at the FN/PEG interface, suggesting that chirality may be in the architecture of the actin filament assembly at the macroscale level, say as clockwise or counterclockwise orientation. Alternatively, it may arise from chirality at the micro- or nanoscale, such as helicity of microfilaments, or chiral rotagen molecules, such as dynein or myosin, in which a molecular chirality directly drives the LR asymmetry. Given that the chirality at the molecular level may be similar among cell-types, our observation that chirality is cell-type specific, together with findings of Wan *et al*,[32] suggests that the cell-type dependence of right/leftward bias may depend on macroscale cytoskeletal chirality, which may vary with cell-type. Thus, instead of “provoking” the LR asymmetry, the substrate interface may merely amplify the LR asymmetry already present in the cytoskeletal assembly.

On the other hand, the 20° steady-state orientation is an independent phenomenon. The evolution to this orientation may result from equilibrium between competing forces, specifically the lateral movements produced by cellular chirality and the outward movement created by random cell motility. It likely involves a combination of matrix traction, cell migration, intercellular signaling, and intercellular mechanical stress. It is not surprising that cells settle into a specific orientation relative to mechanical signals, given that tissue aligns to mechanical stress *in vivo*, as in skeletal, muscle and vascular tissues. During the subsequent aggregation stage, the observed coherent migration into patterns of multicellular aggregates may involve both reaction-diffusion and matrix traction.[33] Given that mechanical inductions introduced from native tissue architecture are lost when cells are enzymatically harvested, our findings may explain why chirality is rarely seen in cultured adult cells.

Cellular LR asymmetry is believed to amplify into tissue LR asymmetry through various means, such as planar cell polarity, an epithelial patterning phenomenon that involves asymmetric distribution of proteins and cross-talk via the cytoskeleton, which determine the apical-basal axis in tissues.[7] *In vivo* examples include drosophila hindgut rotation[8] and the coherent orientation of cardiomyocytes, which form individual concentric layers of fibers, with incrementally increasing angle in each layer from the epicardium to the endocardium.[34] At a broader level, this robust capacity of differentiated cells to self-organize into multicellular structures with LR asymmetric alignment may have a fundamental role in embryogenesis and postnatal development, allowing cell-based engineering of regenerative tissues that are architecturally and functionally more authentic than previously possible.

Supplementary Material

Refer to Web version on PubMed Central for supplementary material.

Acknowledgments

We thank A. P. Sage, Xingjuan Zeng and J. Lu for scientific discussion and technical assistance.

Sources of Funding

This research was supported by grants from the National Science Foundation (SINAM 00006047 and BECS EFRI-1025073) and the National Institutes of Health (HL081202 and DK081346). C. Guo, Z. Li and X. Zhao were supported by grants from National Natural Science Foundation of China (NSFC/60875059, 91023045) and National High Technology Research and Development Program of China (863 program/2009AA043703).

Non-standard Abbreviations and Acronyms

LR	Left-right
VMC	Vascular mesenchymal cell
HMDS	Hexamethyldisilazane
PEG	Polyethylene glycol
ECM	Extracellular matrix
FN	Fibronectin
BVEC	Bovine vascular endothelial cell
3T3	NIH 3T3 fibroblast
ST2	Mouse bone marrow stromal cell line
BMP-2	Bone morphogenetic protein-2
GFP	Green fluorescent protein
CCD	Charge-coupled device
NMM-IIa	Non-muscle myosin-IIa
MGP	Matrix gamma-carboxyglutamic acid protein
MTOC	Microtubule organizing center

References

1. Okumura T, Utsuno H, Kuroda J, Gittenberger E, Asami T, Matsuno K. The Development and Evolution of Left-Right Asymmetry in Invertebrates: Lessons From Drosophila and Snails. Dev Dyn. 2008; 237:3497–3515. [PubMed: 19035360]
2. Aw S, Levin M. Is left-right asymmetry a form of planar cell polarity? Development. 2009; 136:355–366. [PubMed: 19141667]
3. Hashimoto M, Shinohara K, Wang J, Ikeuchi S, Yoshiba S, Meno C, Nonaka S, Takada S, Hatta K, Wynshaw-Boris A, Hamada H. Planar polarization of node cells determines the rotational axis of node cilia. Nat Cell Biol. 2010; 12:170–176. [PubMed: 20098415]
4. Song H, Hu J, Chen W, Elliott G, Andre P, Gao B, Yang Y. Planar cell polarity breaks bilateral symmetry by controlling ciliary positioning. Nature. 2010; 466:378–382. [PubMed: 20562861]
5. Danilchik MV, Brown EE, Riegert K. Intrinsic chiral properties of the Xenopus egg cortex: an early indicator of left-right asymmetry? Development. 2006; 133:4517–4526. [PubMed: 17050623]
6. Pohl C, Bao Z. Chiral Forces Organize Left-Right Patterning in C. elegans by Uncoupling Midline and Anteroposterior Axis. Dev Cell. 2010; 19:402–412. [PubMed: 20833362]

7. Aw S, Levin M. What's Left in Asymmetry? Dev Dyn. 2008; 237:3453–3463. [PubMed: 18488999]
8. Taniguchi K, Maeda R, Ando T, Okumura T, Nakazawa N, Hatori R, Nakamura M, Hozumi S, Fujiwara H, Matsuno K. Chirality in Planar Cell Shape Contributes to Left-Right Asymmetric Epithelial Morphogenesis. Science. 2011; 333:339–341. [PubMed: 21764746]
9. Bostrom K, Watson KE, Horn S, Wortham C, Herman IM, Demer LL. Bone Morphogenetic Protein Expression in Human Atherosclerotic Lesions. J Clin Invest. 1993; 91:1800–1809. [PubMed: 8473518]
10. Hsiai TK, Cho SK, Reddy S, Hama S, Navab M, Demer LL, Honda HM, Ho CM. Pulsatile flow regulates monocyte adhesion to oxidized lipid-induced endothelial cells. Arterioscler Thromb Vasc Biol. 2001; 21:1770–1776. [PubMed: 11701464]
11. Wong PK, Yu F, Shahangian A, Cheng G, Sun R, Ho C-M. Closed-loop control of cellular functions using combinatory drugs guided by a stochastic search algorithm. Proc Natl Acad Sci U S A. 2008; 105:5105–5110. [PubMed: 18356295]
12. Farrington-Rock C, Crofts NJ, Doherty MJ, Ashton BA, Griffin-Jones C, Canfield AE. Chondrogenic and adipogenic potential of microvascular pericytes. Circulation. 2004; 110:2226–2232. [PubMed: 15466630]
13. Cheng S-L, Shao J-S, Charlton-Kachigian N, Loewy AP, Towler DA. Msx2 promotes osteogenesis and suppresses adipogenic differentiation of multipotent mesenchymal progenitors. J Biol Chem. 2003; 278:45969–45977. [PubMed: 12925529]
14. Garfinkel A, Tintut Y, Petrasek D, Bostrom K, Demer LL. Pattern formation by vascular mesenchymal cells. Proc Natl Acad Sci U S A. 2004; 101:9247–9250. [PubMed: 15197273]
15. Turing AM. The Chemical Basis of Morphogenesis. Philos Trans R Soc Lond B Biol Sci. 1952; 237:37–72.
16. Tintut Y, Alfonso Z, Saini T, Radcliff K, Watson K, Bostrom K, Demer LL. Multilineage potential of cells from the artery wall. Circulation. 2003; 108:2505–2510. [PubMed: 14581408]
17. Li N, Ho C-M. Photolithographic patterning of organosilane monolayer for generating large area two-dimensional B lymphocyte arrays. Lab Chip. 2008; 8:2105–2112. [PubMed: 19023473]
18. Maini PK, McElwain DLS, Leavesley DI. Traveling wave model to interpret a wound-healing cell migration assay for human peritoneal mesothelial cells. Tissue Eng. 2004; 10:475–482. [PubMed: 15165464]
19. Painter KJ, Maini PK, Othmer HG. Stripe formation in juvenile Pomacanthus explained by a generalized Turing mechanism with chemotaxis. Proc Natl Acad Sci U S A. 1999; 96:5549–5554. [PubMed: 10318921]
20. DiMilla PA, Quinn JA, Albelda SM, Lauffenburger DA. Measurement of Individual Cell Migration Parameters for Human Tissue Cells. AIChE Journal. 1992; 38:1092–1104.
21. Witkin, A.; Kass, M. Reaction-Diffusion Textures.; Paper presented at: SIGGRAPH Computer Graphics; Las Vegas, NV, USA. July, 1991;
22. Ridley AJ, Schwartz MA, Burridge K, Firtel RA, Ginsberg MH, Borisy G, Parsons JT, Horwitz AR. Cell migration: Integrating signals from front to back. Science. 2003; 302:1704–1709. [PubMed: 14657486]
23. Jiang XY, Bruzewicz DA, Wong AP, Piel M, Whitesides GM. Directing cell migration with asymmetric micropatterns. Proc Natl Acad Sci U S A. 2005; 102:975–978. [PubMed: 15653772]
24. Thery M, Racine V, Piel M, Pepin A, Dimitrov A, Chen Y, Sibarita JB, Bornens M. Anisotropy of cell adhesive microenvironment governs cell internal organization and orientation of polarity. Proc Natl Acad Sci U S A. 2006; 103:19771–19776. [PubMed: 17179050]
25. Desai RA, Gao L, Raghavan S, Liu WF, Chen CS. Cell polarity triggered by cell-cell adhesion via E-cadherin. J Cell Sci. 2009; 122:905–911. [PubMed: 19258396]
26. Palazzo AF, Joseph HL, Chen Y-J, Dujardin DL, Alberts AS, Pfister KK, Vallee RB, Gundersen GG. Cdc42 dynein, and dynactin regulate MTOC reorientation independent of Rho-regulated microtubule stabilization. Curr Biol. 2001; 11:1536–1541. [PubMed: 11591323]
27. Conti MA, Adelstein RS. Nonmuscle myosin II moves in new directions. J Cell Sci. 2008; 121:11–18. [PubMed: 18096687]
28. Kilian KA, Bugarija B, Lahn BT, Mrksich M. Geometric cues for directing the differentiation of mesenchymal stem cells. Proc Natl Acad Sci U S A. 2010; 107:4872–4877. [PubMed: 20194780]

29. Nelson CM, Jean RP, Tan JL, Liu WF, Sniadecki NJ, Spector AA, Chen CS. Emergent patterns of growth controlled by multicellular form and mechanics. Proc Natl Acad Sci U S A. 2005; 102:11594–11599. [PubMed: 16049098]

30. Engler AJ, Sen S, Sweeney HL, Discher DE. Matrix elasticity directs stem cell lineage specification. Cell. 2006; 126:677–689. [PubMed: 16923388]

31. Xu J, Van Keymeulen A, Wakida NM, Carlton P, Berns MW, Bourne HR. Polarity reveals intrinsic cell chirality. Proc Natl Acad Sci U S A. 2007; 104:9296–9300. [PubMed: 17517645]

32. Wan LQ, Ronaldson K, Park M, Taylor G, Zhang Y, Gimble JM, Vunjak-Novakovic G. Micropatterned mammalian cells exhibit phenotype-specific left-right asymmetry. Proc Natl Acad Sci U S A. 2011; 108:12295–12300. [PubMed: 21709270]

33. Maruthamuthu V, Sabass B, Schwarz US, Gardel ML. Cell-ECM traction force modulates endogenous tension at cell-cell contacts. Proc Natl Acad Sci U S A. 2011; 108:4708–4713. [PubMed: 21383129]

34. Streeter DD, Spotnitz HM, Patel DP, Ross J, H. SE. Fiber Orientation in Canine Left Ventricle during Diastole and Systole. Circ Res. 1969; 24:339–347. [PubMed: 5766515]

Novelty and Significance

What is known?

- The emergence of left-right asymmetry is a critical step in tissue morphogenesis.
- This asymmetry has been attributed to a hypothetical innate cellular chirality, and pattern formation has been attributed to reaction-diffusion phenomena.
- Left-right asymmetry is rarely observed in conventional cell culture.

What new information does this article contribute?

- Vascular mesenchymal cells preferentially turn right on migration across an unbiased substrate interface and then orient at 20° to the interface.
- In the presence of multiple parallel interfaces, they further self-organize into parallel diagonal stripes evenly spaced throughout the culture.
- This rightward bias requires accumulation of stress fibers at the interface, suggesting that mechanical signals play a critical role in this asymmetric morphogenesis.

Summary Paragraph

It is not clear how cells distinguish left *vs*. right to produce tissue and organ asymmetry. We have found that vascular cells encountering a substrate interface preferentially turn right and that, with multiple interfaces, they self-organize into a regular diagonal patterns of macroscopic stripes. In this manner, asymmetry in cells may be translated and amplified into a *de novo* LR asymmetry at the tissue level. This LR-bias required stress fiber accumulation in cells at the interface, potentially explaining the lack of LR asymmetry in conventional cultures where substrate interfaces, such as those in our experiments and in nature, are absent. This phenomenon may be a simple model for the left-right asymmetry seen in the spatial plan of many organs. In addition to serving as a model of how tissue is laid out in development, these findings offer novel mechanisms of cellular self-organization and may guide cell-based therapy for tissue repair.

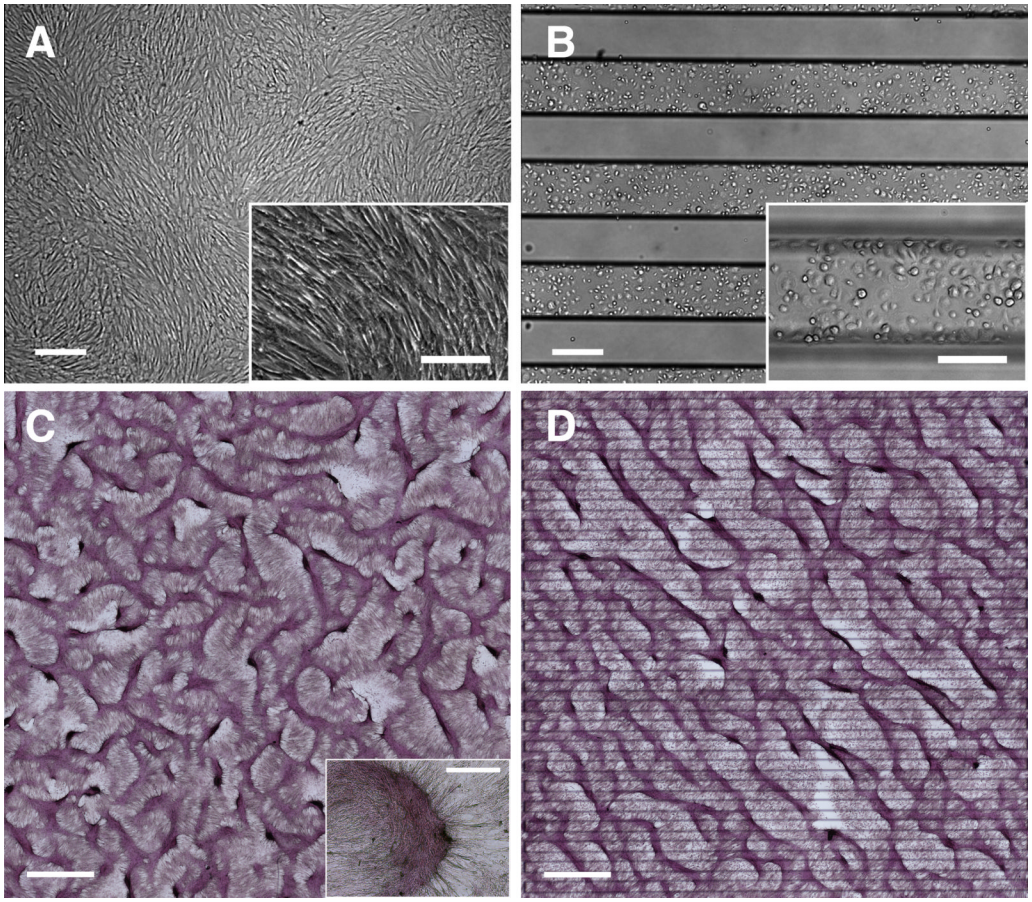

Figure 1. LR asymmetry in pattern formation by vascular mesenchymal cells

Phase contrast microscopy of VMCs on (**A**) conventional plastic substrate at confluence and (**B**) FN/PEG substrates (interfaces identified by black titanium lines) showing preferential attachment to FN domain immediately after plating. Scale bar, 300 μm and 200 μm (inset). After 10-14 days, development of regularly spaced aggregates (**C**) in a labyrinthine configuration and (**D**) in a stripe pattern along principal diagonal axis in bright field (multicellular ridges stained with hematoxylin). Insets: higher magnification images of multicellular aggregates. Scale bar, 2 mm and 300 μm (inset).

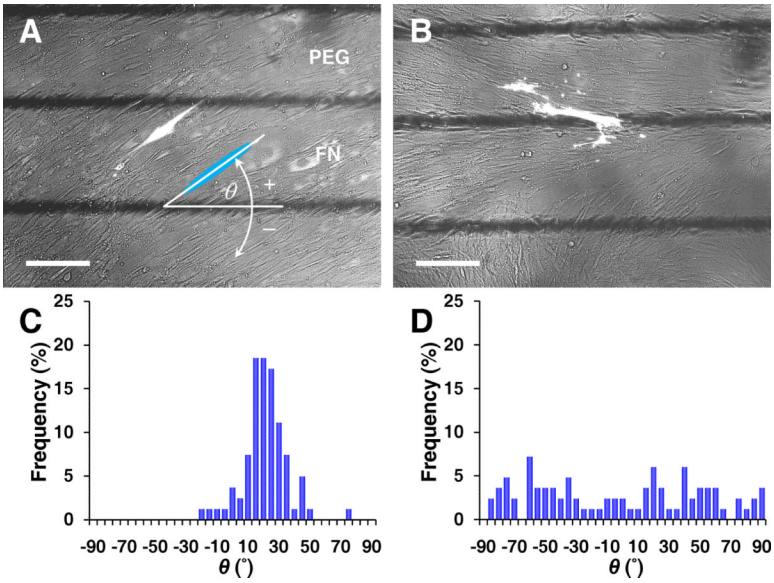

Figure 2. Early stage of coherent single-cell orientation perpendicular to the axis of diagonal ridges

Fluorescence microscopy of GFP-transfected VMCs on (**A**) FN/PEG substrates showing coherent individual cell orientation, relative to the interface axis (black lines) and (**B**) control substrate as homogeneous FN. Scale bar, 200 μm. Histogram of θ for (**C**) FN/PEG, showing convergence to 19 ± 14° (n = 81 cells; day 5; mean ± s.d.) and (**D**) control substrate, showing non-convergence (n = 83 cells; day 5).

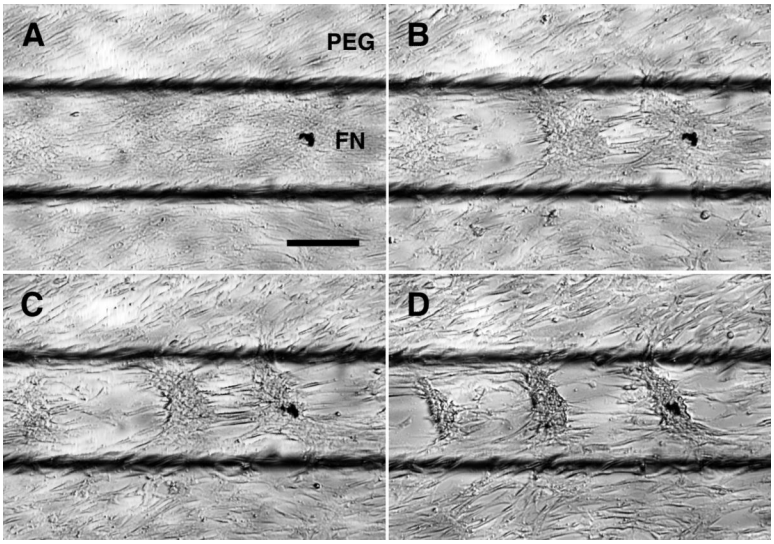

Figure 3. Cell migration toward aggregates directed by the coherent orientation

Time-lapse videomicroscopic images at (**A**) $t = 0$, (**B**) $t = 150$, (**C**) $t = 300$, and (**D**) $t = 625$ min. Scale bar, 200 μm.

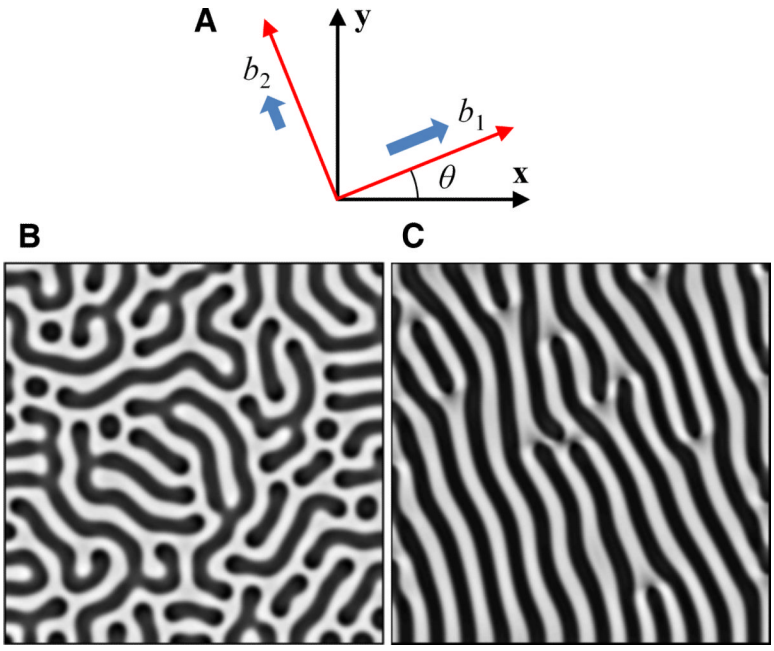

Figure 4. Numerical simulations showing that the anisotropic migration leads to parallel ridges with asymmetric alignment

A, Schematic of coefficients, b_1 and b_2, for principal directions of anisotropic migration. Simulation results for $n(x, y)$ with darker areas representing higher density yielded (**B**) a labyrinthine pattern at steady state for isotropic migration ($b_1 = b_2 = 1$) and (**C**) an asymmetric pattern for anisotropic migration ($b_1 = 1$, $b_2 = 10^{-6}$). Model parameters: $D = 0.005$, $\gamma = 20000$, $k = 0.28$, $c = 0.01$, $e = 0.02$, $D_n = 0.06$, $\chi_0 = 0.06$, $k_n = 1$, $\theta = 20°$, $r = 322$, $t^* = 1$ (total time).

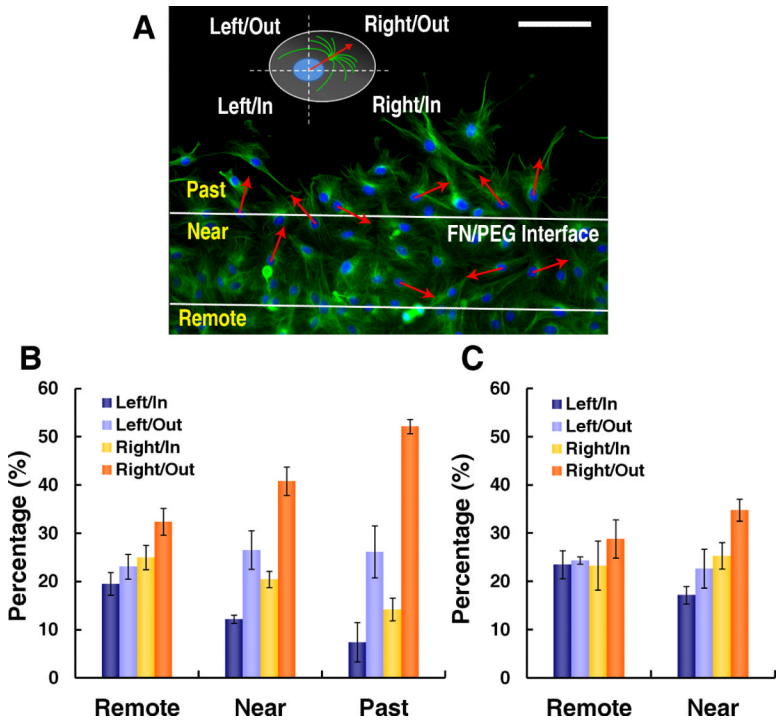

Figure 5. LR polarity at FN/PEG interface

A, Immunofluorescence microscopy of α-tubulin in VMCs on FN/PEG with polarity defined based on MTOC orientation relative to nuclear centroid and interface for cells past, near, and 120 μm remote from interface. Scale bar, 100 μm. VMC polarity (**B**) 6 hours after plating (n = 3 experiments; > 370 cells each; mean ± s.d.) and (**C**) 2 hours after plating (n = 3 experiments; > 260 cells each; mean ± s.d.).

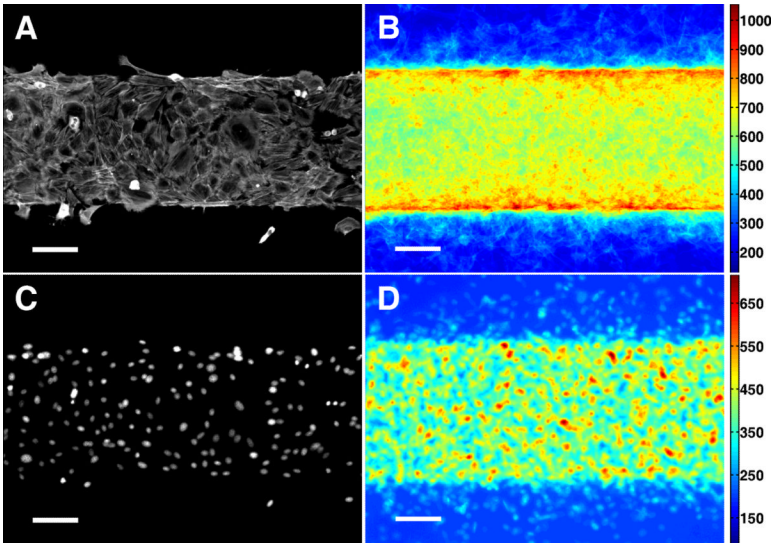

Figure 6. Stress fiber accumulation at FN/PEG interface

Immunofluorescence microscopy of NMM-IIa in VMCs on FN/PEG substrate shown as (**A**) a single image and (**B**) stacked images (n = 45). Immunofluorescence microscopy of nuclei of VMCs on FN/PEG substrate shown as (**C**) a single image and (**D**) stacked images (n = 45). Scale bar, 100 μm.

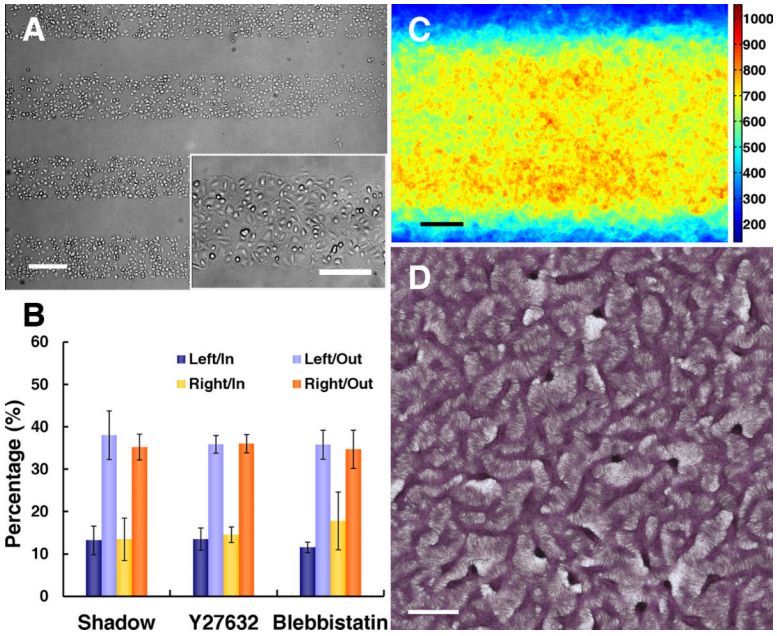

Figure 7. Abrogation of LR polarity and LR alignment of multicellular ridges with removal of substrate interfaces

A, Microscopic images after shadow-mask plating show plating limited to rectangular domains. Scale bar, 300 μm and 200 μm (inset). **B**, Polarity of VMCs at the edges of cell sheets shadow-plated onto uniform FN (n = 3 experiments; > 175 cells each; mean ± s.d.) and VMCs near the FN/PEG interface with Y27632 (n = 3; > 135 cells each) or blebbistatin (n = 3; > 150 cells each) inhibition. **C**, Stacked images of NMM-IIa immunofluorescence after shadow-plating on FN (n = 40). Scale bar, 100 μm. **D**, Multicellular patterns by hematoxylin staining after shadow-plating on FN substrate. Scale bar, 2 mm.

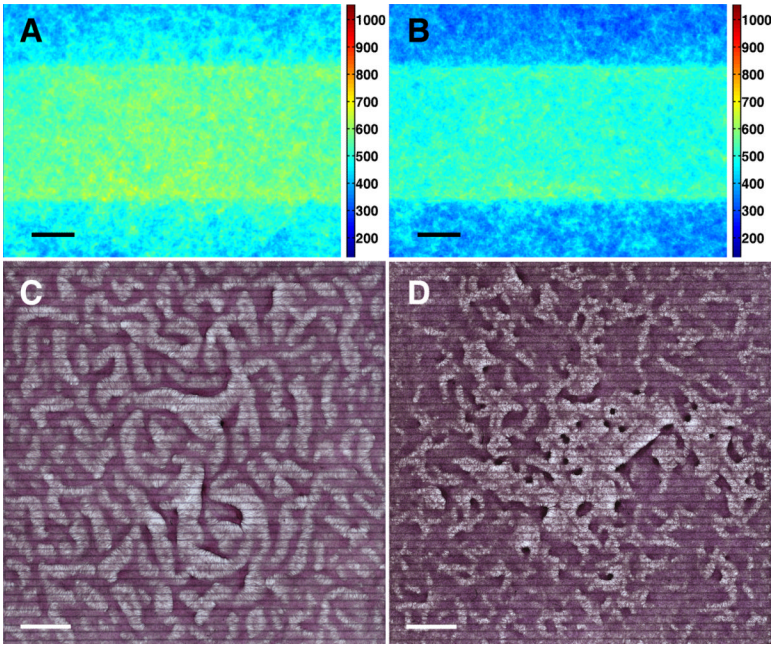

Figure 8. Abrogation of LR alignment of multicellular ridges with stress fiber inhibition

Stacked images of NMM-IIa immunofluorescence (**A**) with Y27632 on FN/PEG substrate (n = 60), and (**B**) with blebbistatin on FN/PEG substrate (n= 45). Scale bar, 100 μm. Multicellular patterns by hematoxylin staining (**C**) with Y27632 on FN/PEG substrate, and (**D**) with blebbistatin on FN/PEG substrate. Scale bar, 2 mm.